THE JOURNAL OF BIOLOGICAL CHEMISTRY VOL. 284, NO. 50, pp. 35079–35091, December 11, 2009

RNA Helicase Prp43 and Its Co-factor Pfa1 Promote 20 to 18 S rRNA Processing Catalyzed by the Endonuclease Nob1[S]

Received for publication, July 6, 2009, and in revised form, September 29, 2009 Published, JBC Papers in Press, September 29, 2009, DOI 10.1074/jbc.M109.040774

Brigitte Pertschy[‡1], Claudia Schneider[§2], Marén Gnädig[‡], Thorsten Schäfer[‡], David Tollervey[§], and Ed Hurt[‡3]

From the [‡]Biochemie-Zentrum der Universität Heidelberg, Im Neuenheimer Feld 328, 69120 Heidelberg, Germany and the [§]Wellcome Trust Centre for Cell Biology, University of Edinburgh, Edinburgh EH9 3JR, Scotland, United Kingdom

Many RNA nucleases and helicases participate in ribosome biogenesis, but how they cooperate with each other is largely unknown. Here we report that *in vivo* cleavage of the yeast pre-rRNA at site D, the 3′-end of the 18 S rRNA, requires functional interactions between PIN (PilT N terminus) domain protein Nob1 and the DEAH box RNA helicase Prp43. Nob1 showed specific cleavage on a D-site substrate analogue *in vitro*, which was abolished by mutations in the Nob1 PIN domain or the RNA substrate. Genetic analyses linked Nob1 to the late pre-40 S-associated factor Ltv1, the RNA helicase Prp43, and its cofactor Pfa1. In strains lacking Ltv1, mutation of Prp43 or Pfa1 led to a striking accumulation of 20 S pre-rRNA in the cytoplasm due to inhibition of site D cleavage. This phenotype was suppressed by increased dosage of wild-type Nob1 but not by Nob1 variants mutated in the catalytic site. In *ltv1/pfa1* mutants the 20 S pre-rRNA was susceptible to 3′ to 5′ degradation by the cytoplasmic exosome. This degraded into the 3′ region of the 18 S rRNA, strongly indicating that the pre-ribosomes are structurally defective.

Eukaryotic ribosome formation is a complex process that requires coordination of rRNA synthesis and processing with the subsequent incorporation of the ribosomal (Rpl and Rps) proteins (reviewed in Refs. 1–5). In the yeast *Saccharomyces cerevisiae*, ribosome synthesis starts with the transcription of a 35 S pre-rRNA, which is the common precursor to the mature 18, 5.8, and 25 S rRNAs. This pre-rRNA is co-transcriptionally bound by ribosomal proteins as well as many non-ribosomal *trans*-acting factors to form a 90 S preribosomal particle. Next, this 90 S intermediate undergoes a series of early pre-rRNA processing and modification steps in the nucleolus before an endonucleolytic cleavage at site A_2 in the pre-rRNA separates the pathways for 60 and 40 S subunit assembly.

Pre-60 S particles undergo further maturation steps in the nucleus, whereas pre-40 S particles contain few non-ribosomal proteins and are rapidly exported to the cytoplasm. The factors involved in 40 S export are largely unknown, but the non-essential pre-40 S factor Ltv1 was suggested to play a role in this process (6). Following nuclear export, the pre-40 S subunit undergoes cytoplasmic maturation, involving two major events. (i) 20 S pre-rRNA cleavage at site D generates the 3′-end of the mature 18 S rRNA, and (ii) structural reorganization forms the characteristic beak structure of the mature 40 S subunit, resulting in exposure of RNA helix 33 within the 18 S rRNA (7).

The sites and the order of endonuclease and exonuclease processing events that convert the 35 S pre-rRNA into the mature rRNA species are well characterized in yeast (Fig. 3*A*) (reviewed in Refs. 4 and 8). However, although most or all of the exonucleases participating in rRNA processing are known, several predicted endonucleases remain to be identified. Two proteins, Fap7 and Nob1, were proposed to cleave site D (9–11), but for neither was endonuclease activity shown. Fap7 is a putative NTPase that transiently associates with preribosomes, whereas Nob1 is a PilT N terminus (PIN)[4] domain protein that stably associates with late pre-40 S particles (10–12). Several proteins were recently shown to have endonuclease activity that was dependent on an intact PIN (13–18) domain.

Assembly of preribosomes also involves 19 putative ATP-dependent RNA helicases. When considering the highly structured nature of the rRNA, the requirement of RNA helicases in ribosome biogenesis could involve the conformational rearrangement of RNA secondary structures, recruitment of additional factors, release of small nucleolar RNAs and proteins from the preribosomal RNAs, or stimulation of endo- and exonuclease activities (19). The direct substrates of the RNA helicases in ribosome biogenesis are largely unknown, and for only few of them (Dbp3, Dbp4, Mtr4, and Rok1) possible substrates were suggested (20–23).

Here, we report that the late pre-40 S factor Ltv1 is genetically linked to the RNA helicase Prp43, its co-factor Pfa1/Sqs1 (24), and to Nob1. 20 to 18 S rRNA processing was strongly impaired in double mutants between *ltv1* and *prp43* or *ltv1* and *pfa1*. However, this defect was rescued by overexpression of Nob1. To test if Nob1 is the D-site-specific RNA processing enzyme, we developed an *in vitro* assay using a model RNA substrate. Nob1 purified from yeast exhibited highly specific endonuclease activity, cleaving precisely at the location corresponding to cleavage site D. Our data indicate that Prp43 and

[S] The on-line version of this article (available at http://www.jbc.org) contains supplemental Tables S1 and S2 and Figs. S1–S4.

[1] Recipient of an Erwin Schrödinger Fellowship from the Austrian Science Fund (FWF; J2612). Present address: Institut für Molekulare Biowissenschaften, Universität Graz, Humboldtstrasse 50, 8010 Graz, Austria.

[2] Supported by a long term fellowship of the Human Frontiers Science Program and by the Wellcome Trust.

[3] Recipient of grants from the Deutsche Forschungsgemeinschaft (Hu363/9-2 and the Gottfried Wilhelm Leibniz Program) and Fonds der Chemischen Industrie. To whom correspondence should be addressed. Tel.: 49-6221-54-4173; Fax: 49-6221-54-4369; E-mail: ed.hurt@bzh.uni-heidelberg.de.

[4] The abbreviations used are: PIN, PilT N terminus; MOPS, 4-morpholinepropanesulfonic acid; ProtA, protein A; SDC, synthetic dextrose complete; TAP, tandem affinity purification; TEV, tobacco etch virus.

Pfa1 act together with Ltv1 to promote D-site cleavage by the endonuclease Nob1.

EXPERIMENTAL PROCEDURES

Yeast Strains and Plasmids—Yeast strains used in this study are listed in supplemental Table S1. Deletion disruption and C-terminal tagging at the genomic locus were performed as described previously (25–27). The synthetic lethal screen with the *ltv1*Δ strain based on red/white colony sectoring was performed at 30 °C as described previously (28). Site-directed mutagenesis of Nob1 was performed by fusion PCR. All cloned DNA fragments generated by PCR amplification were verified by sequencing. Plasmids used in this study are listed in supplemental Table S2.

Fluorescence in Situ Hybridization—Fluorescence *in situ* hybridization was carried out as described previously (29), using a Cy3-labeled ITS1 (internal transcribed spacer)-specific probe (5′-Cy3-ATG CTC TTG CCA AAA CAA AAA AAT CCA TTT TCA AAA TTA TTA AAT TTC TT-3′) for detection of ITS1-containing pre-rRNAs. Cells were examined by fluorescence microscopy using an Imager Z1 microscope (Carl Zeiss) with a ×100, numerical aperture 1.4 Plan-Apo-Chromat oil immersion lens and a DICIII, 4′,6-diamidino-2-phenylindole, or HECy3 filter, respectively.

Sucrose Gradient Analysis and Fractionation—Cell extracts for polysome profile analyses were prepared as described previously (30). Sucrose gradients were analyzed and fractionated using an UA-6 system (Teledyne ISCO) with continuous monitoring at $A_{254\,nm}$. For Northern analysis of sucrose gradient fractions, six $A_{260\,nm}$ units of cell extract were layered onto 7–50% sucrose gradients, and the gradients were centrifuged at 38,000 rpm in a SW40 rotor (Beckman Coulter) for 4 h and 30 min. Fractions were collected and adjusted to 10 mM Tris-HCl, pH 7.5, 10 mM EDTA, 0.5% SDS, and RNA was extracted with phenol/chloroform/isoamyl alcohol (25:24:1; two times) and chloroform/isoamyl alcohol (24:1), followed by ethanol precipitation.

RNA Isolation and Northern Blotting—Total RNA preparations were performed from 40 A_{600} units using the mechanical disruption protocol of the RNeasy minikit (Qiagen). 3 μg of RNA per sample were separated on 1.5% MOPS-agarose gels as described in the manual for the RNeasy minikit. The RNA was transferred overnight onto a Hybond N nylon membrane (Amersham Biosciences) and afterward cross-linked to the membrane by UV. RNA on the membrane was stained with 0.02% methylene blue (in 0.3 M sodium acetate, pH 5.5). Hybridization was done overnight at 42 °C in 500 mM $NaPO_4$ buffer, pH 7.2, 7% SDS, 1 mM EDTA using 5′-^{32}P-labeled oligonucleotides with the following sequences: D/A2, 5′-GAC TCT CCA TCT CTT GTC TTC TTG-3′; E/C2, 5′-GGC CAG CAA TTT CAA GTT A-3′; 25 S, 5′-CTC CGC TTA TTG ATA TGC-3′; 18 S-5′, 5′-CAT GGC TTA ATC TTT GAG AC-3′; 18 S (006), 5′-GTA CTA GCG ACG GGC GGT GTG-3′; 18 S (007), 5′-GCG GTG TGT ACA AAG GGC AG-3′. The membranes were washed three times for 20 min at 42 °C in 40 mM $NaPO_4$ buffer, pH 7.2, 1% SDS, and radioactivity was detected by exposing x-ray films. Membranes were regenerated by washing in 1% SDS.

Tandem Affinity Purification (TAP) and Mass Spectrometry—TAP purifications of TAP-tagged bait proteins were, unless otherwise indicated, performed in a buffer containing 50 mM Tris-HCl, pH 7.5, 100 mM NaCl, 1.5 mM $MgCl_2$, and 0.075% Nonidet P-40 essentially as described previously (27). Tobacco etch virus (TEV) protease was preincubated with RiboLock RNase inhibitor (Fermentas), and for cleavage, dithiothreitol was added to a final concentration of 1 mM to the buffer. For analysis of the protein composition of the purified material, the eluates were trichloroacetic acid-precipitated and dissolved in SDS sample buffer. The samples were then separated on NuPAGE SDS 4–12% gradient polyacrylamide gels (Invitrogen) and stained with colloidal Coomassie (Sigma). Mass spectrometric identification of the proteins contained in Coomassie-stained bands was performed as described previously (31). RNA extractions from the eluates were performed as described above for sucrose gradient analysis.

Preparation of Total Yeast Protein Extracts and Western Analysis—Total yeast protein extracts were prepared as described previously (32). Western blot analysis was performed using the following antibodies: anti-Arc1 (1:20,000) (33) and secondary goat anti-rabbit horseradish peroxidase-conjugated antibody (1:7,500) (Bio-Rad); anti-FLAG monoclonal, peroxidase-conjugated (1:1,000; Sigma). For detection of Protein A-tagged proteins, the peroxidase anti-peroxidase complex antibody was used at a dilution of 1:10,000 (Dako). Proteins were visualized using enhanced chemiluminescence detection kits (Immobilon Western (Millipore) and Amersham Biosciences ECL (GE Healthcare)).

Nob1 Purification for Nuclease Assays—For the nuclease assays, ProtA-TEV-FLAG-Nob1 wild type and D15N were expressed in yeast from plasmids pADH111-ProtA-TEV-FLAG-Nob1 or pADH111-ProtA-TEV-FLAG-Nob1-D15N (*ADH1* promoter). Because a *nob1* D15N mutant is not viable (Fig. 9*A*), we overexpressed the protein in a strain that still contained the wild-type copy of the protein. Because we noticed that Nob1 forms multimers and wild-type Nob1 co-purified with the D15N mutant (data not shown), we used a His_6-tagged wild-type copy that was under the control of a *GAL* promoter (pRS313 pGAL-His6-Nob1) when purifying the D15N mutant protein. Cells were grown to an A_{600} of 0.2 in synthetic medium containing 2% raffinose and 0.2% galactose to avoid overexpression of wild-type Nob1 from the *GAL* promoter. Subsequently, expression of the wild-type Nob1 protein was repressed by adding glucose to a final concentration of 2%. Cells were depleted of wild-type Nob1 for ~20 h and harvested at an A_{600} of 2. Cells expressing the wild-type Nob1 protein were grown in glucose-containing synthetic medium and also harvested at an A_{600} of 2. Proteins were affinity-purified using a buffer containing 750 mM NaCl, 50 mM Tris-HCl, pH 7.5, 1.5 mM $MgCl_2$, and 0.075% Nonidet P-40. Briefly, cells were lysed by bead beating (Pulverisette 6, Fritsch) and Nob1 was bound to IgG-Sepharose (Amersham Biosciences) via the ProtA tag. IgG slurry was washed, and proteins were eluted by cleavage with the TEV-protease and incubated with anti-FLAG M2-agarose (Sigma). Anti-FLAG slurry was washed, and the bound material was eluted with FLAG peptide according to the manufacturer's instructions (Sigma). To remove residual His_6-Nob1, the eluates were incubated with Ni^{2+}-ni-

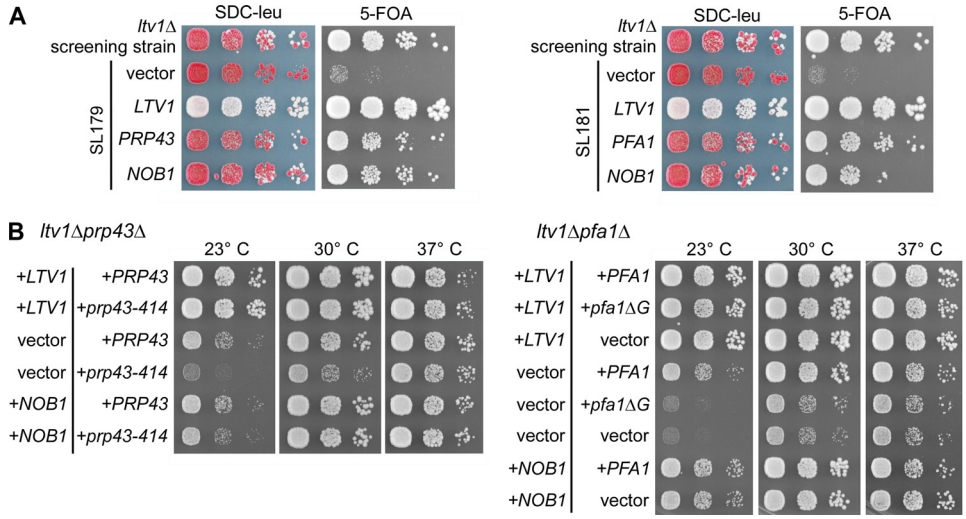

FIGURE 1. **Genetic network between *LTV1*, *PRP43*, *PFA1*, and *NOB1*.** *A*, identification of *PRP43*, *PFA1*, and *NOB1* in a synthetic lethal screen with an *ltv1* deletion strain. Mutants SL179 and SL181 isolated in the synthetic lethal (*sl*) screen were transformed with plasmids carrying the indicated genes and spotted in serial 10-fold dilution steps onto SDC−leu and SDC + 5-fluoroorotic acid (*5-FOA*) plates. As control, the non-mutagenized screening strain (*ltv1*Δ, pHT4467-CENΔ-*LTV1*) was spotted. Plates were incubated at 30 °C for 4 days. Red colony color on SDC−leu and slow growth on 5-fluoroorotic acid plates indicate a synthetic growth defect. Red/white sectoring on SDC−leu and growth on 5-fluoroorotic acid indicate complementation of the synthetic enhancement phenotype. *B*, temperature dependence of genetic interactions between *LTV1* and *PRP43* and between *LTV1* and *PFA1*. The *LTV1/PFA1* and *LTV1/PRP43* shuffle strains were transformed with plasmids that carry the indicated wild-type and mutant alleles. *pfa1ΔG* is a *PFA1* allele lacking the G-patch. After 5-fluoroorotic acid shuffling, cells were spotted in 10-fold serial dilution steps onto SDC−leu−trp plates to select for the transformed plasmids and incubated at 23, 30, and 37 °C for 4 days.

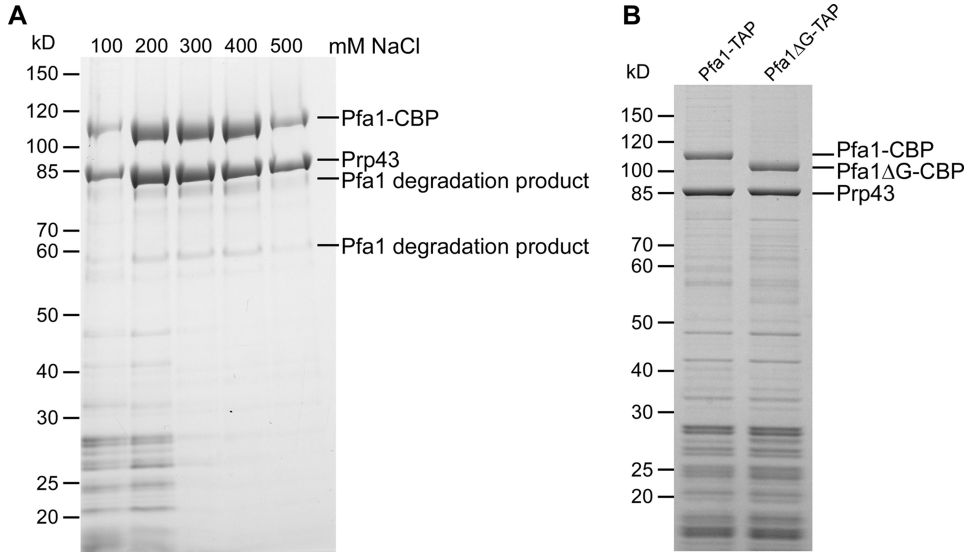

FIGURE 2. **The interaction between Prp43 and Pfa1 is independent of the G-patch and resistant to increased salt concentrations.** *A*, Pfa1-TAP was purified from yeast cells using increasing salt concentrations, ranging from 100 to 500 mM NaCl. Samples were analyzed by SDS-PAGE and Coomassie staining. The indicated proteins were identified by mass spectrometry. Note that at higher salt concentrations, only Pfa1 (full-length and degradation products) and Prp43 were recovered, indicating that Pfa1 and Prp43 directly interact *in vivo*. *Pfa1-CBP*, Pfa1 with the C-terminal calmodulin-binding protein tag. *B*, Pfa1- and Pfa1ΔG-TAP purifications. Note that the C-terminally truncated version of Pfa1 co-purified amounts of Prp43 similar to those provided by the full-length protein. All bands appearing in only one of the two purifications could be identified by mass spectrometry as N-terminal degradation products of Pfa1 that differed in size due to the different C termini of the bait proteins.

trilotriacetic acid-agarose (Qiagen) in the presence of 10 mM imidazole. The unbound material was concentrated, and the buffer was exchanged into (150 mM NaCl, 50 mM Tris-HCl, 0.5 mM dithiothreitol, 10% glycerol) on Ultrafree-0.5 centrifugal filter devices (10K NMWL, Millipore).

In Vitro Nuclease Assays—Nuclease activity tests of wild-type or mutant (D15N) Nob1 proteins purified from yeast (see above) on 5′-radiolabeled RNAs were performed at 30 °C in 25 mM Tris/HCl (pH 7.6), 75 mM NaCl, 2 mM dithiothreitol, 100 μg/ml bovine serum albumin, 0.8 unit/μl RNasin, 4.5% glycerol, 0.05% Nonidet P-40, 0.3 μM *Escherichia coli* tRNA. Unless otherwise indicated, 5 mM $MnCl_2$ was used. Prior to the addition of the labeled RNA substrate, the 10-μl reactions containing the protein were preincubated for 5 min at 30 °C and then subsequently (unless otherwise indicated) incubated for 60 min at 30 °C in the presence of the RNA. After a proteinase K digest for 30 min at 37 °C, the RNA was then extracted, precipitated, and resuspended in formamide RNA loading buffer. Reaction products were resolved on a denaturing 12% polyacrylamide, 8 M urea gel and visualized by autoradiography.

5′-End-labeled substrates were stem D-site WT or stem D-site "U17G" RNAs (see Fig. 7*B*; Dharmacon). 5′-End labeling and gel purification of the labeled RNAs was performed as described (34).

RESULTS

A Genetic Network between the Pre-40 S Factor Ltv1, the RNA Helicase Prp43, the G-patch Protein Pfa1, and the Nuclease Nob1—Ltv1 is a non-essential component of late pre-40 S particles that also contain Enp1, Hrr25, Nob1, Rio2, Tsr1, Dim1, and Dim2 (7). Within this particle, Ltv1 forms a stable complex with Enp1 and the ribosomal protein Rps3, which was previously proposed to be involved in 40 S beak formation (7). To identify pre-40 S factors that functionally interact with Ltv1, we performed a synthetic lethal screen with a strain harboring the *ltv1* null allele. Haploid *ltv1*Δ cells are viable and exhibit only a slight growth impairment at 23 or 30 °C (Fig. 1). Our screen was performed at 30 °C, and eight mutants were identified that exhibited a synthetic enhanced phenotype in combination with deletion of *LTV1*.

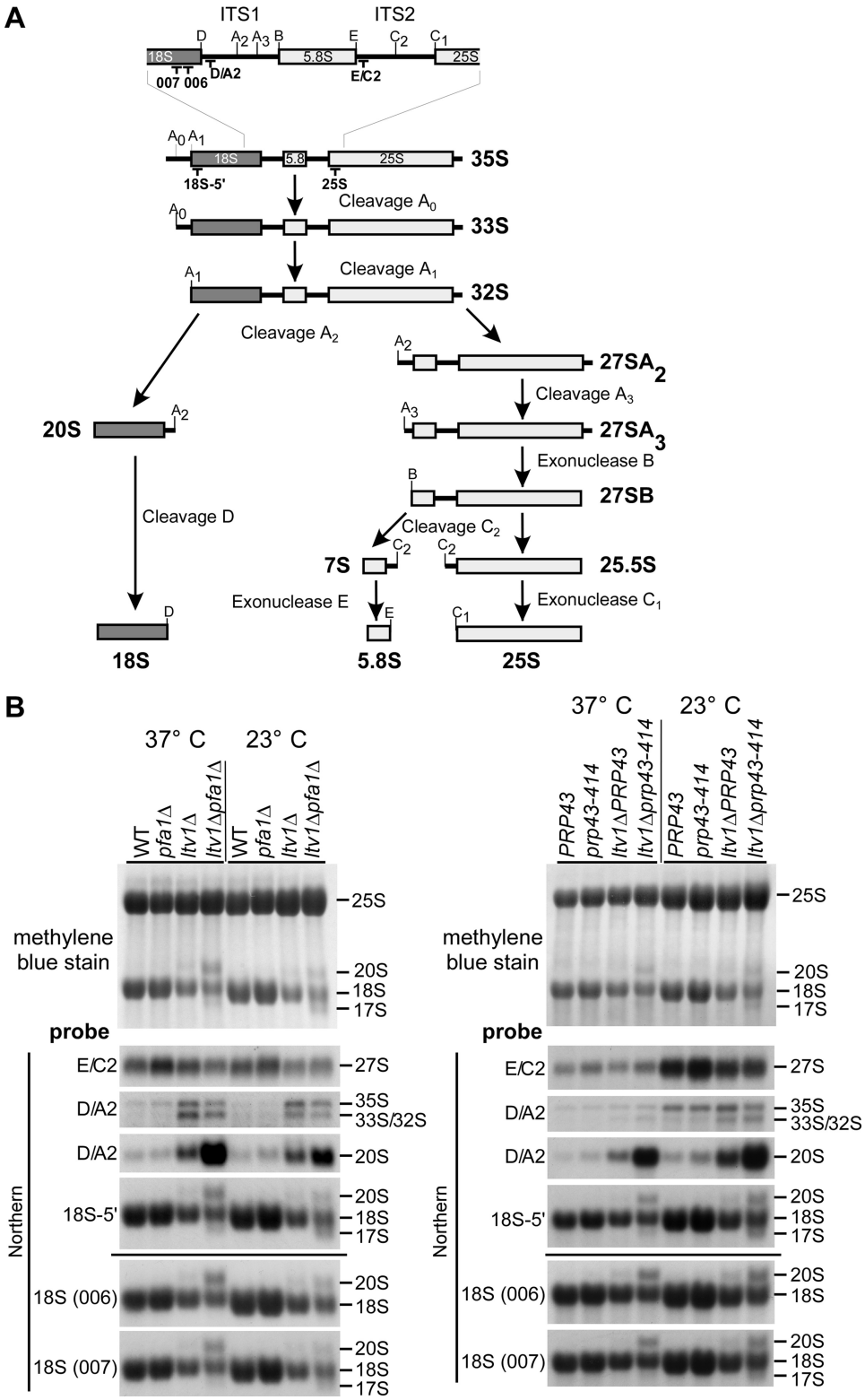

FIGURE 3. **Ltv1, Pfa1, and Prp43 are required for 20 to 18 S rRNA processing.** *A*, simplified rRNA processing pathway in yeast. Only the major pathway for generation of the 5′-end of the 5.8 S rRNA is shown. The rRNA cleavage sites and the binding sites of the probes used for Northern blotting are indicated. ITS1 and ITS2, internal transcribed spacers 1 and 2. In the course of pre-rRNA processing, the 35 S pre-rRNA undergoes a series of endonucleolytic processing events at sites A_0, A_1, and A_2 that lead to the separation into the 20 S and 27 S A_2 pre-rRNAs. Endo- and exonucleolytic processing steps of the 27 S A_2 pre-rRNA finally yield the mature 25 and 5.8 S rRNAs contained in 60 S subunits. In the cytoplasm, the final processing step in 40 S maturation takes place when the 20 S pre-rRNA is converted into the 18 S rRNA by endonucleolytic cleavage at processing site D. *B*, rRNA steady state levels in *ltv1*Δ *pfa1*Δ and *ltv1*Δ *prp43–414* mutants. Cells were either grown at 37 °C to an A_{600} of 0.8 (37 °C) or grown at 37 °C to an A_{600} of 0.1, transferred to 23 °C, and further grown to an A_{600} of 0.8 (three cell divisions). RNA was isolated, separated by agarose gel electrophoresis, and transferred to a nylon membrane that was stained with methylene blue. rRNA processing intermediates were detected by Northern blotting using the indicated probes. *WT*, wild type.

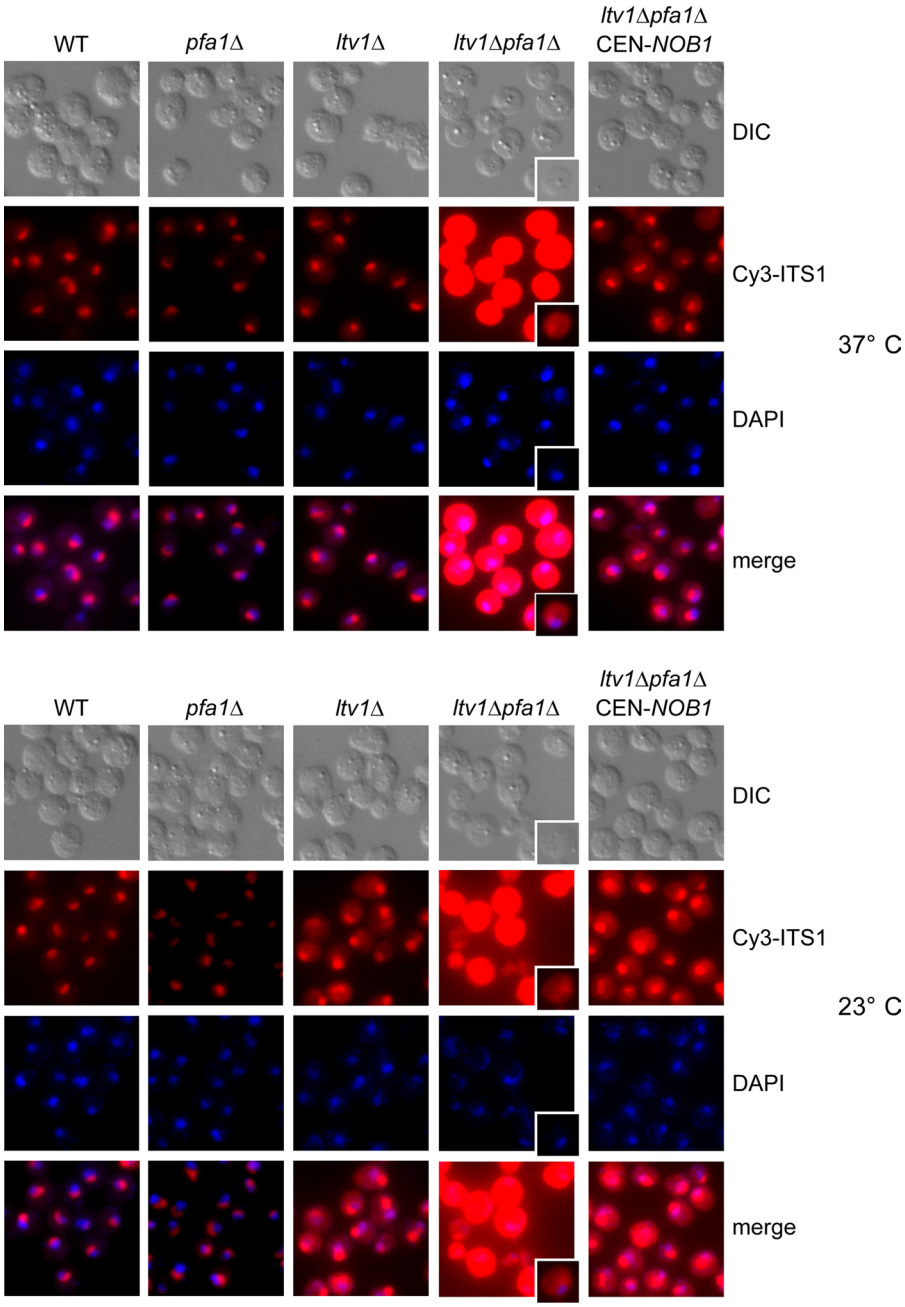

FIGURE 4. **20 S pre-rRNA accumulates in the cytoplasm in *ltv1*Δ *pfa1*Δ mutants.** *ltv1*Δ *pfa1*Δ cells transformed with empty plasmids or plasmids carrying *LTV1*, *PFA1*, or *NOB1* wild-type alleles were either grown at 37 °C to an A_{600} of 0.7–1 (37 °C) or grown to an A_{600} of 0.3, and shifted to 23 °C for 3 h (23 °C). Cells were fixed with formaldehyde, spheroplasted, and subjected to fluorescence *in situ* hybridization using a Cy3-labeled probe complementary to a sequence in the D/A2 segment of ITS1. To visualize the nucleoplasm, cells were stained with 4′,6-diamidino-2-phenylindole (*DAPI*). Due to the strong signal in the *ltv1*Δ *pfa1*Δ cells, also single cells with a shorter exposure of the Cy3 signal are shown. *WT*, wild type.

mutations in the non-essential gene *PFA1* (data not shown). In addition, synthetic growth inhibition was also observed between *ltv1*Δ and other *prp43* mutant alleles mapping in several different motifs of the helicase fold (data not shown). Subsequently, the synthetic enhanced genetic interactions were verified by generating the corresponding double mutants, *ltv1*Δ *prp43–414* and *ltv1*Δ *pfa1*Δ (Fig. 1*B*). Notably, the synthetic growth defects, which were very pronounced at 23 °C, were gradually reduced at higher temperatures (Fig. 1*B*, compare 23, 30, and 37 °C). As predicted from the genetic screen, the presence of the *NOB1* gene on a centromeric plasmid was sufficient to suppress the synthetic enhanced growth phenotypes of both double mutant strains (Fig. 1*B*). Altogether, these data suggest that *ltv1*Δ exhibits a synthetic enhanced genetic interaction with *PRP43* and *PFA1* that is suppressed by increased dosage of Nob1.

The DEAH-box RNA helicase Prp43 is a characterized splicing factor (35, 36) and is also required for early steps in ribosome biogenesis (24, 37, 38) and for the release of small nucleolar RNAs from the pre-60 S ribosomes (39). Prp43 is associated with several pre-rRNAs, including 20 S (24, 37, 38), and binds the pre-rRNA at multiple sites, including 18 S helix 44, close to cleavage site D (39). In the splicing pathway, Prp43 forms a complex with the G-patch protein Ntr1/Spp382 that stimulates its helicase activity (40–42). The G-patch domain is an ~50-amino acid-long motif that is found in several proteins linked to RNA processing (43). Two other G-patch proteins, Pxr1/Gno1 and Pfa1/Sqs1, were reported to interact with Prp43 (24). The interaction between Prp43 and Pfa1 is most likely direct, because both proteins can be co-purified from yeast in a salt-resistant complex that is stable even after treatment with RNase A (Fig. 2*A*) (data not shown). Moreover, the G-patch domain of Pfa1 is of functional importance, because expression of Pfa1 lacking this motif (Pfa1ΔG) did not complement the growth defect of the *ltv1*Δ *pfa1*Δ mutant (Fig. 1*B*). This truncated version of Pfa1 was expressed similarly to the full-length protein and was still able to interact with Prp43, suggesting that removal of the G-patch dis-

After transformation with a genomic library, we found that one of these mutants (SL179) was complemented by either *NOB1* or *PRP43*, whereas the other seven mutants (including SL181) were complemented by either *NOB1* or *PFA1/SQS1* (Fig. 1*A*). DNA sequencing revealed that the *NOB1* gene locus was not mutated in any of these synthetic enhanced mutants. SL179 carried a point mutation in *PRP43* corresponding to a S414F amino acid exchange in the sequence between helicase motifs V and VI of the protein (hereafter referred to as *prp43–414*). The remaining seven synthetic enhanced strains carried

turbs a function of Pfa1 other than interaction with Prp43 (Fig. 2*B*) (data not shown). By analogy to the helicase-activating function of Ntr1, our data suggest that the G-patch of Pfa1 might stimulate Prp43 helicase activity during a late step in 40 S subunit biogenesis.

Ltv1, Prp43, and Pfa1 Are Required for 20 to 18 S rRNA Processing in the Cytoplasm—To investigate whether Pfa1 and Prp43, in conjunction with Ltv1, control the late 20 to 18 S rRNA processing step in the cytoplasm, we performed Northern analyses using the probes depicted in Fig. 3*A*. Robust accumulation of 20 S pre-rRNA and concomitant reduction in mature 18 S rRNA was observed in the *ltv1*Δ *pfa1*Δ and *ltv1*Δ *prp43–414* double mutants, whereas the single mutants were unaffected (*pfa1*Δ and *prp43–414*) or only slightly impaired (*ltv1*Δ) in this processing step (Fig. 3*B*). Unexpectedly, although the synergistic growth defects of the double mutants were less obvious at 37 °C (see Fig. 1*B*), 20 S pre-rRNA accumulation was even stronger at 37 °C than at 23 °C (Fig. 3*B*; see also "Discussion").

To determine where 20 S pre-rRNA accumulated in the double mutants, we performed *in situ* hybridization using a fluorescently labeled oligonucleotide complementary to a sequence between cleavage sites D and A2 in ITS1. This probe detects the 20 S pre-rRNA and larger precursors but not mature 18 S rRNA (Fig. 3*A*). Consistent with the Northern data, the *ltv1*Δ *pfa1*Δ and *ltv1*Δ *prp43–414* double mutants, but not the single mutants, massively accumulated pre-rRNAs harboring ITS1 in the cytoplasm at both 37 and 23 °C (Fig. 4 and supplemental Fig. S1). Shorter exposure also revealed some ITS1 accumulation in the nucleolus (Fig. 4). This could, however, be due to increased levels of 35 S and 32/33 S pre-rRNAs in these mutants, which were clearly visible in the Northern analysis (Fig. 3*B*). Notably, the strong cytoplasmic ITS1 signal and the accumulation of 20 S pre-rRNA and an abnormal 17 S RNA species (see below) could be reverted by increasing the dosage of Nob1 (Figs. 4 and 9*C*). Together, these studies demonstrate that combined mutations in *LTV1* and *PFA1* or *LTV1* and *PRP43* cause a robust inhibition of cytoplasmic 20 to 18 S rRNA processing, which can be suppressed by overexpression of Nob1.

*An Abnormal 17 S RNA Product Generated by the Exosome Is Formed in ltv1*Δ *pfa1*Δ *and ltv1*Δ *prp43–414 Double Mutants*—In addition to the 20 S pre-rRNA, we observed the formation of a 17 S RNA species in the *ltv1*Δ *pfa1*Δ and *ltv1*Δ *prp43–414* double mutants (Figs. 3*B* and 6 and supplemental Fig. S2). As shown by using specific Northern probes (see Figs. 3*A* and 10*A*), this abnormal 17 S RNA species is a 3′-truncated form of 18 S rRNA that was already described in *rps14* and *fap7* mutants (9, 44). Notably, the 17 S RNA accumulated more strongly at 23 °C than at 37 °C in the *ltv1*Δ *pfa1*Δ and *ltv1*Δ *prp43–414* double mutants (Fig. 3*B*).

To determine whether the 17 S RNA was generated by endonuclease or exonuclease activity in the double mutants, we first searched for a hypothetical rRNA endonuclease cleavage product extending from the 3′-end of the 17 S RNA to cleavage site A2 by Northern analysis. However, we could not detect such a fragment even in a strain lacking the 5′–3′ exonuclease XrnI, which is responsible for degradation of the D/A2 spacer fragment generated by 20 S cleavage (data not shown) (45). We next tested whether the 3′ to 5′ exonuclease activity of the cytoplasmic exosome is involved in generating the 17 S RNA. Loss of cofactors for the cytoplasmic exosome Ski2 or Ski7 (46, 47) from the *ltv1*Δ *pfa1*Δ strain abolished formation of 17 S RNA, whereas levels of 20 S pre-rRNA were significantly increased (Fig. 5*A*). This suggests that the 17 S RNA was predominantly derived from 20 S pre-rRNA, although it remains possible that some 17 S RNA can be generated from mature 18 S rRNA. Ski2, Ski7, and the cytoplasmic exosome participate in several mRNA degradation pathways but were not previously reported to process or degrade rRNAs (reviewed in Ref. 48).

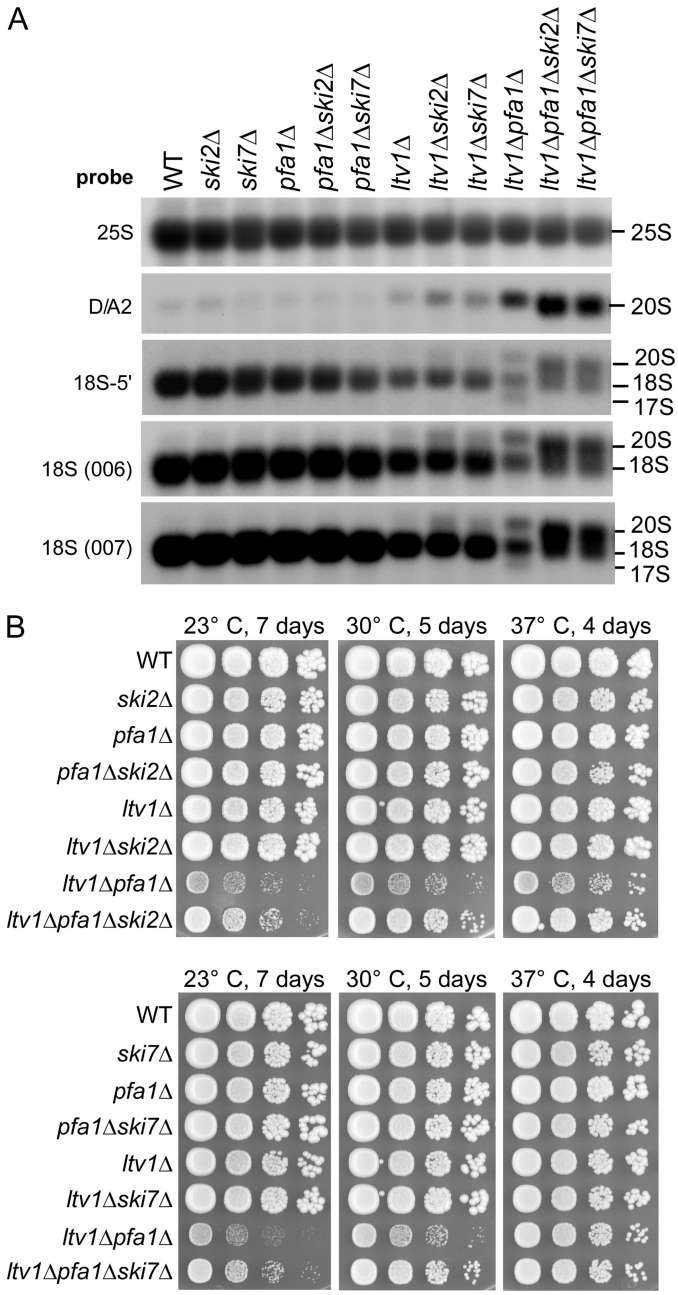

FIGURE 5. **17 S RNA is generated via an 3′–5′ exonucleolytic attack by the exosome.** *A*, the abnormal 17 S RNA species is not formed when *SKI2* or *SKI7* is deleted. Cells were grown at 30 °C to an A_{600} of 0.8. RNA was isolated and analyzed by Northern blotting using the indicated probes. *B*, *ltv1*Δ *pfa1*Δ mutants grow faster when also *SKI2* or *SKI7* is deleted. Growth of *ski2*Δ (*top*) and *ski7*Δ (*bottom*) mutants is shown. Cells were spotted in 10-fold serial dilution steps onto YPD plates and incubated at the indicated temperatures for the indicated time periods. *WT*, wild type.

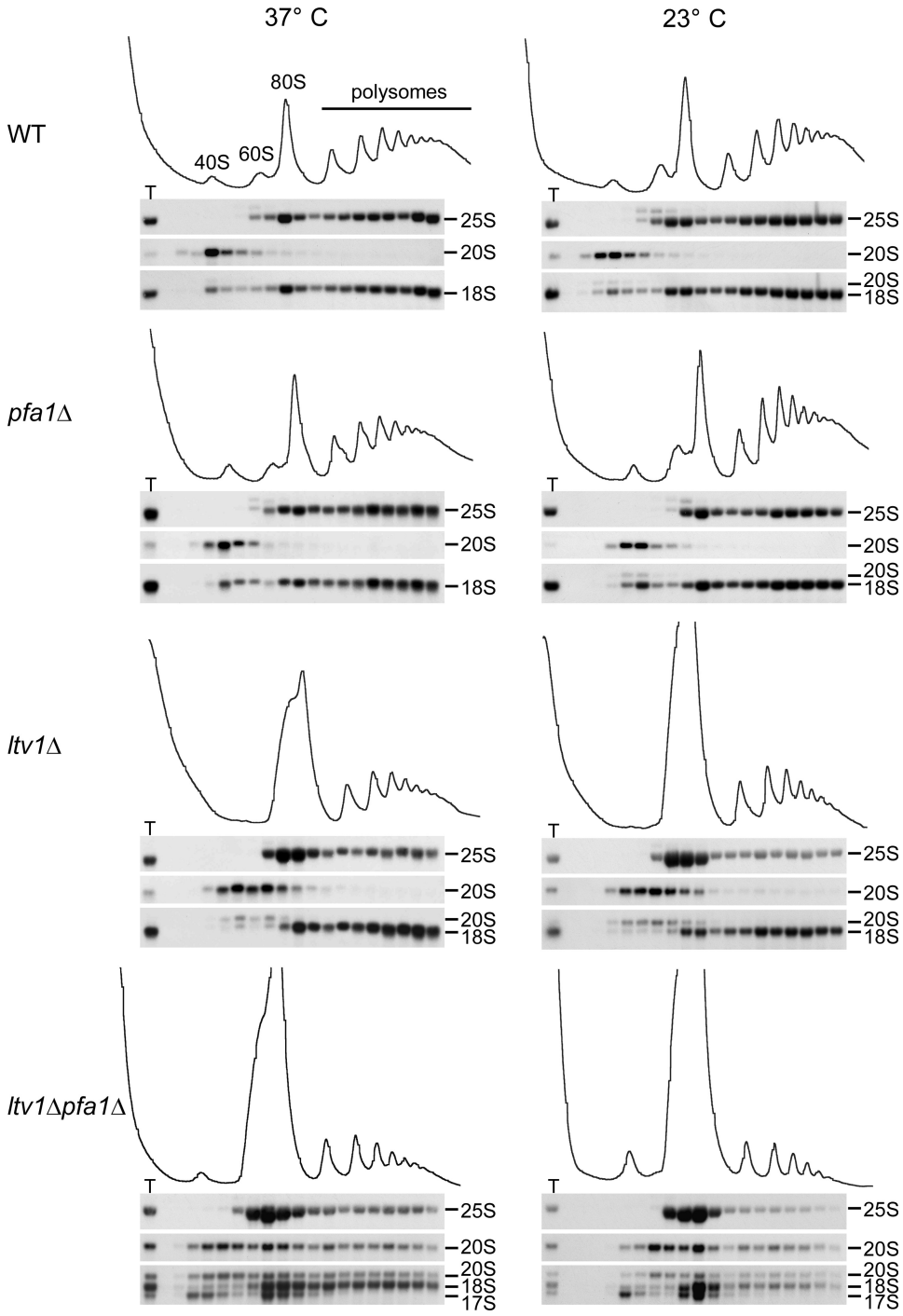

FIGURE 6. **17 S RNA co-sediments only with 40 and 80 S, whereas 20 S pre-rRNA is also found in polysomes.** Cells were either grown at 37 °C to an A_{600} of 0.7–1 (37 °C) or grown to an A_{600} of 0.1, shifted to 23 °C, and incubated to an A_{600} of 0.7–1 (23 °C). Cell extracts were loaded onto 7–50% sucrose gradients and fractionated. RNA was extracted from each fraction and analyzed by Northern blotting using the probes 25 S, D/A2 (to detect 20 S pre-rRNA), and 5′-18 S (to detect 20, 18, and 17 S rRNAs). *T*, RNA preparation of the total extract. *WT*, wild type.

Analysis of the *ltv1*Δ *pfa1*Δ and *ltv1*Δ *prp43–414* double mutants by sucrose density gradient centrifugation showed reduced levels of polysomes and 40 S subunits, whereas 60 and 80 S peaks were increased (Fig. 6 and supplemental Fig. S2). Subsequent Northern analysis of these fractions showed that 20, 18, and 17 S rRNAs were prominently enriched in the area corresponding to the 80 S peak. Notably, 20 S pre-rRNA was not only found in the 40 and 80 S peak but also in the polysomal fractions, implying that it may be present in functional polysomes. In contrast, 17 S RNA was not detected in the polysomal fractions, suggesting that 40 S subunits containing 17 S RNA are non-functional. Consistent with this hypothesis, the abundance of free 60 S subunits was reduced in an *ltv1*Δ *pfa1*Δ *ski2*Δ triple mutant as compared with the *ltv1*Δ *pfa1*Δ strain, suggesting that more 40 S subunits are capable of subunit joining when 17 S RNA formation is prevented (supplemental Fig. S3). Furthermore, *ltv1*Δ *pfa1*Δ mutants grew faster when *SKI2* or *SKI7* were also deleted, showing that the 17 S RNA accumulation and therefore the presence of aberrant 40 S subunits accounts for part of the growth defect observed in *ltv1*Δ *pfa1*Δ double mutants (Fig. 5*B*; also see "Discussion").

Nob1 Has D-site-specific Endonuclease Activity in Vitro—Increased dosage of Nob1 suppressed both the slow growth phenotype (Fig. 1) and the 20 S pre-rRNA accumulation (Figs. 4 and 9*C* and supplemental Fig. S1) of the *ltv1*Δ *pfa1*Δ and *ltv1*Δ *prp43–414* double mutants. This suggested that Nob1 participated directly in pre-rRNA cleavage at site D. Hence, we tested whether Nob1 exhibits *in vitro* site D cleavage activity.

To obtain purified Nob1, we first tested recombinant expression in *E. coli* but failed to obtain pure and soluble protein. We then overexpressed ProtA-FLAG-tagged Nob1 in yeast and affinity-purified it under stringent, high salt conditions (Fig. 7*A*). As a control, we also affinity-purified a mutant Nob1-D15N protein, in which the catalytic nuclease activity of the PIN domain was predicted to be destroyed (10, 11). Since the Nob1-D15N mutant on its own does not support growth (Fig. 9*A*), it was expressed in a strain in which the endogenous *NOB1* gene was under *GAL* regulation (for details regarding the purification procedure, see "Experimental Procedures"). When analyzed by SDS-PAGE and Coomassie staining, purified wild-type and mutant Nob1 proteins exhibited several bands. The major bands between 50 and 60 kDa were identified by mass spectrometry to be Nob1.

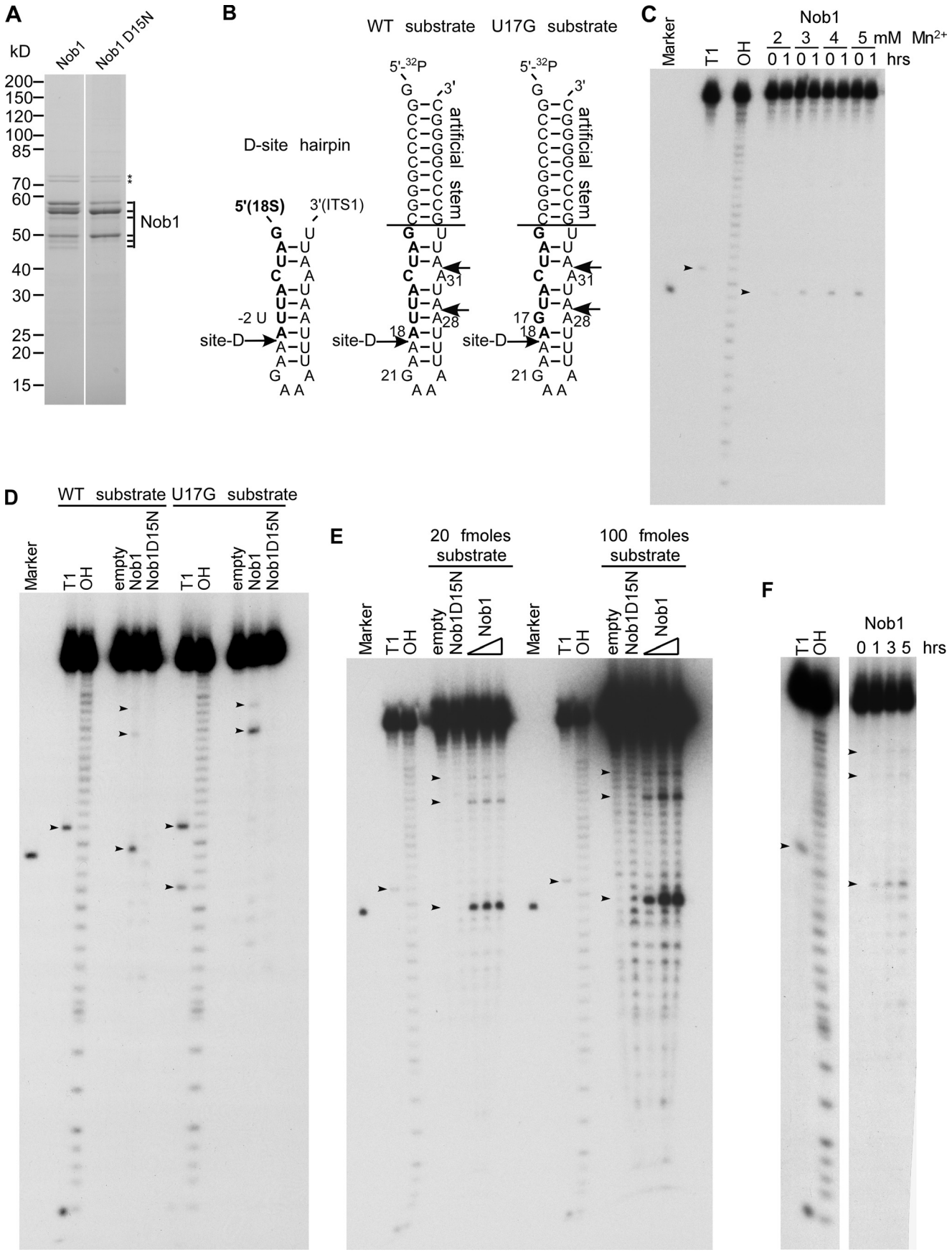
A
kD
Nob1
Nob1 D15N
200
150
120
100
85
70
60
50
40
30
25
20
15
**
Nob1
B
WT substrate
U17G substrate
5'-32P
3'
artificial stem
D-site hairpin
5'(18S)
3'(ITS1)
site-D
-2 U
18
21 G
17 G
C
Marker
T1
OH
Nob1
2 3 4 5 mM Mn2+
0 1 0 1 0 1 0 1 hrs
D
WT substrate
U17G substrate
Marker
T1
OH
empty
Nob1
Nob1D15N
E
20 fmoles substrate
100 fmoles substrate
Marker
T1
OH
empty
Nob1D15N
Nob1
F
T1
OH
Nob1
0 1 3 5 hrs

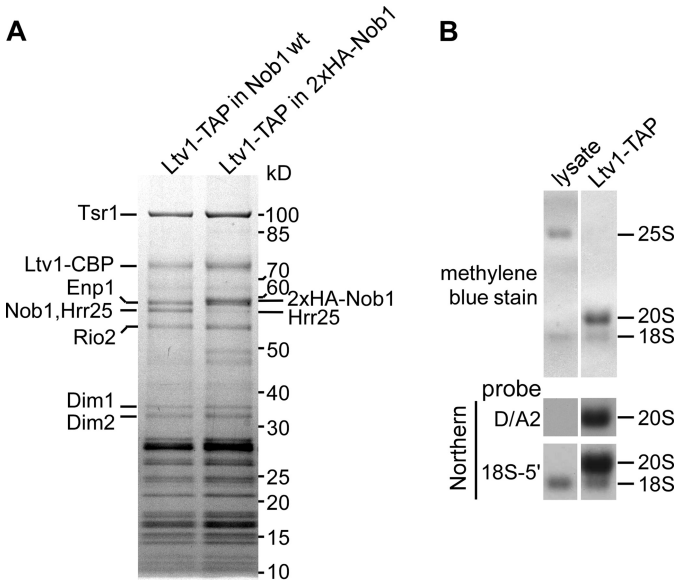

FIGURE 8. **pre-40 S particles purified via Ltv1-TAP contain Nob1 and unprocessed 20 S pre-rRNA.** *A*, Nob1 is stably associated with the pre-40 S particle affinity-purified via Ltv1-TAP. The Ltv1-TAP preparation was analyzed by SDS-PAGE and Coomassie staining. Bands identified by mass spectrometry are indicated. Nob1 and Hrr25 co-migrate as one band. To estimate the proportion of Nob1 in this band, we performed another purification where the size of Nob1 was increased by fusion to an N-terminal hemagglutinin tag. *B*, the main RNA species in the Ltv1-TAP purification is 20 S pre-rRNA. RNA was extracted from the cell lysate and the pre-40 S subunit purified via Ltv1-TAP, separated on an agarose gel and transferred to a nylon membrane that was stained with methylene blue. The 20 and 18 S rRNAs were detected by Northern blotting with specific probes (see Fig. 3*A*).

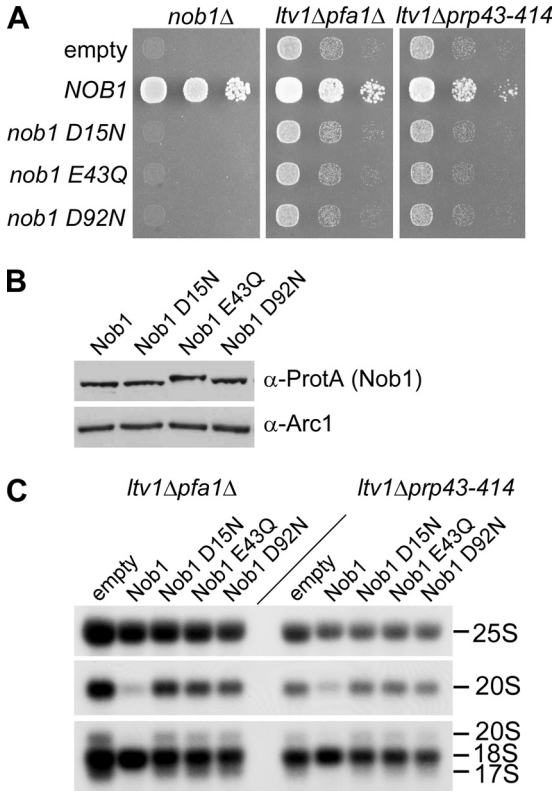

FIGURE 9. **Suppression of the rRNA processing defects in *ltv1Δ pfa1Δ* and *ltv1Δ prp43–414* mutants requires the endonuclease activity of Nob1.** *A*, to test whether the *nob1* mutant alleles are functional *in vivo*, plasmids expressing Nob1 mutants that were N-terminally tagged with ProtA-FLAG were transformed into a *NOB1* shuffle strain, and growth was tested by spotting cells in 10-fold dilution steps onto plates containing 5-fluoroorotic acid (*5-FOA*) and incubated at 30 °C for 2 days. Growth indicates complementation of the *nob1* deletion. To test for suppression, plasmids were transformed into the double mutants *ltv1Δ pfa1Δ* and *ltv1Δ prp43–414*, and transformants were spotted onto SDC−leu plates. Plates were incubated at 30 °C for 4 days. *B*, expression of the indicated Nob1 mutant proteins was tested by analyzing whole cell lysates from a *NOB1* shuffle strain transformed with the respective plasmids and Western blotting against the ProtA tag. The Western blot using an antibody against Arc1 serves as a loading control. Note that the electrophoretic mobility of the mutant variants is slightly changed, which could be due to the removed negative charge. *C*, Northern blotting of *ltv1Δ pfa1Δ* and *ltv1Δ prp43–414* strains transformed with plasmids carrying the indicated ProtA-FLAG-tagged Nob1 variants. Cells were grown at 30 °C to an A_{600} of 0.8. RNA was isolated and analyzed by Northern blotting using the 25 S probe to detect 25 S rRNA, the D/A2 probe to detect 20 S pre-rRNA, and the 18 S 5′ probe to detect 20, 18, and 17 S rRNAs.

Although we cannot fully exclude the possibility that the larger versions are modified forms of Nob1, we consider it unlikely because similar gel migration was observed with protein purified from *E. coli* (data not shown). In addition, mass spectrometric analysis suggested that the band sedimenting at 50 kDa was most likely a C-terminally truncated version of Nob1 (data not shown). For these reasons, we assume that the uppermost band (close to the 60 kDa band of the protein marker) corresponds to full-length Nob1 (with a predicted molecular mass of ~52 kDa) that exhibits a slightly abnormal running behavior, whereas the faster migrating bands are most likely C-terminally

FIGURE 7. **Nob1 has D-site-specific endonuclease activity *in vitro*.** *A*, purified wild-type Nob1 and mutant Nob1-D15N used in the *in vitro* nuclease assay. The proteins were affinity-purified from yeast and analyzed by SDS-PAGE and Coomassie staining. All bands labeled with Nob1 were identified by mass spectrometry. Hsp70 contaminants are indicated by *stars*. *B*, model of the cleavage site D within the 20 S pre-rRNA. *Left sequence*, authentic D-site hairpin ranging from 5′ (part of mature 18 S rRNA; shown in *boldface type*) to 3′ (part of ITS1, shown in *normal type*) (53); *middle* and *right sequences*, RNA model substrates with engineered wild-type (*middle*) and mutated cleavage site D (U17G mutation) (*right*). Both RNA substrates carry an additional stem sequence attached to the D-site hairpin. Alternative cleavage sites at positions A28 and A31 are indicated. *C–F*, Nob1 *in vitro* cleavage assays. *Marker*, 18-nucleotide RNA resembling the expected D-site cleavage product, ranging from nucleotide 1 to 18 of the used WT substrate. *T1*, substrate digested with T1 nuclease, which cleaves after single-stranded G residues (G^1 and G^{21}, as well as G^{17} in the U17G substrate). OH, partial alkaline hydrolysis of the RNA substrate. Due to the generation of 3′-phosphates upon hydrolysis by T1 nuclease or OH^-, the products run slightly faster (~1.5 nucleotides) than cleavage products with 3′-OH ends. 3′-OH ends are found in the marker and in cleavage products predicted to be generated by PIN endonucleases, as shown for the exosome subunit Rrp44 (14). Note that the cleavage product of Nob1 runs at a similar height as the A18 oligonucleotide, indicating that cleavage occurs after A18, corresponding to the D-site. Small variations in cleavage efficiencies in the assays shown are probably due to the use of different protein and/or RNA substrate preparations. *C*, manganese titration. 5′-[^{32}P]-end-labeled RNA substrate was incubated with purified wild-type Nob1 at 30 °C for 0 or 1 h in the presence of increasing concentrations of manganese as indicated. ~5 pmol of Nob1 and 10 fmol of substrate were used (500-fold molar excess). The *arrows* indicate the G^{21} cleavage product generated by T1 nuclease and the A^{18} cleavage product generated by Nob1. *D*, cleavage does not occur when either the catalytic site of Nob1 (Nob1-D15N) or the sequence of the substrate (U17G) is mutated. 10 fmol of 5′-^{32}P-end-labeled RNA substrates (shown in *B*) were incubated without protein (*empty*) or with purified wild-type Nob1 or mutant Nob1-D15N (5 pmol each) at 30 °C for 1 h. The *arrows* indicate the G^{17} and G^{21} cleavage products generated by T1 nuclease and the A^{18}, A^{28}, and A^{31} cleavage products generated by Nob1. *E*, dependence of the cleavage reaction on enzyme and substrate concentration. 20 (*left*) and 100 (*right*) fmol of RNA substrate were incubated with 1.25, 2.5, or 5 pmol of Nob1 protein for 1 h at 30 °C. In the case of the Nob1-D15N protein, 5 pmol were used. The *arrows* indicate the G^{21} cleavage product generated by T1 nuclease and the A^{18}, A^{28}, and A^{31} cleavage products generated by Nob1. *F*, time course of Nob1 cleavage. 20 fmol of substrate were incubated with 10 pmol of Nob1 at 30 °C for the indicated time periods. The *arrows* indicate the G^{21} cleavage product generated by T1 nuclease and the A^{18}, A^{28}, and A^{31} cleavage products generated by Nob1. *WT*, wild type.

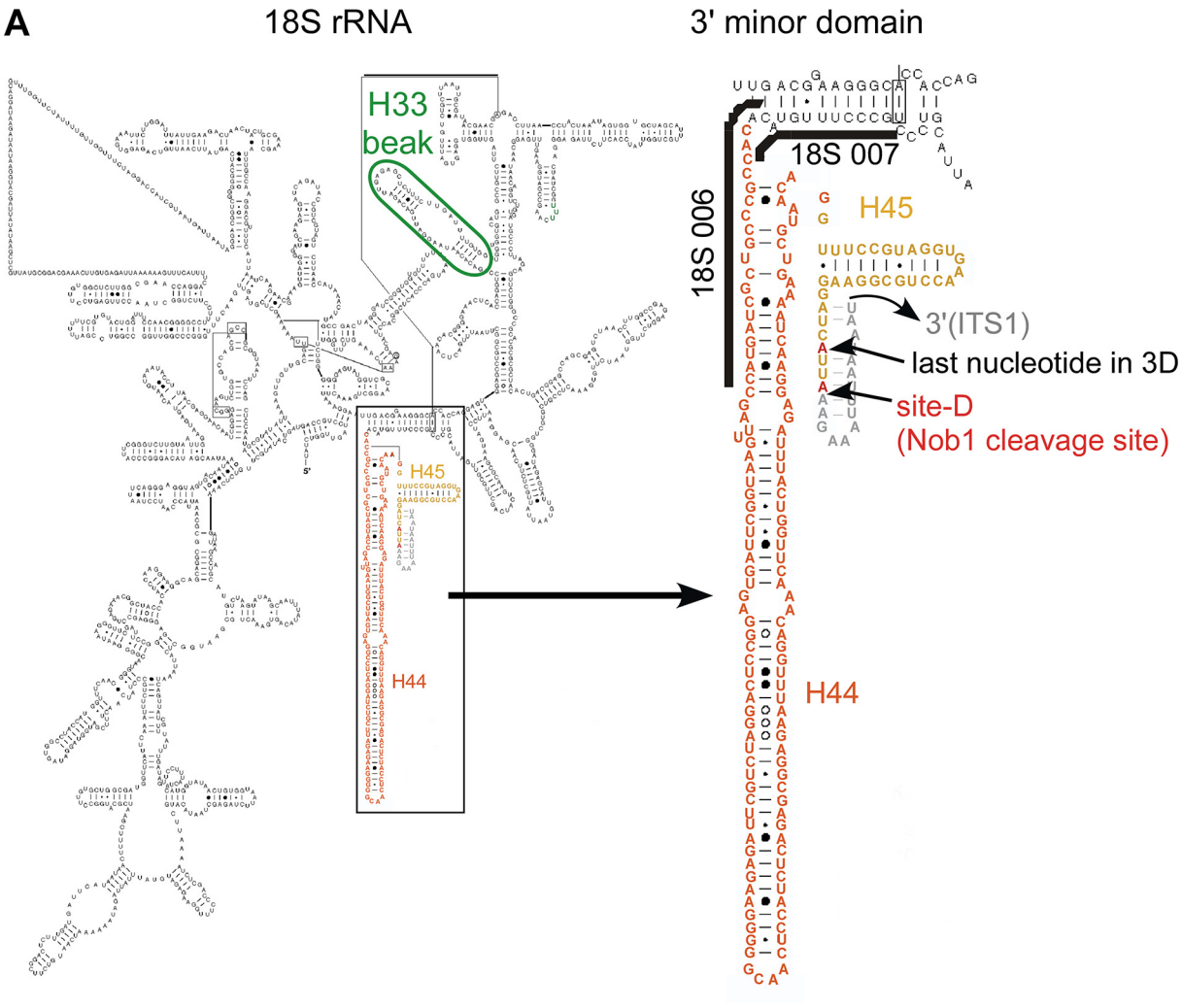
A
18S rRNA
3' minor domain
H33
beak
H45
H44
18S 007
18S 006
H45
3'(ITS1)
last nucleotide in 3D
site-D
(Nob1 cleavage site)
H44

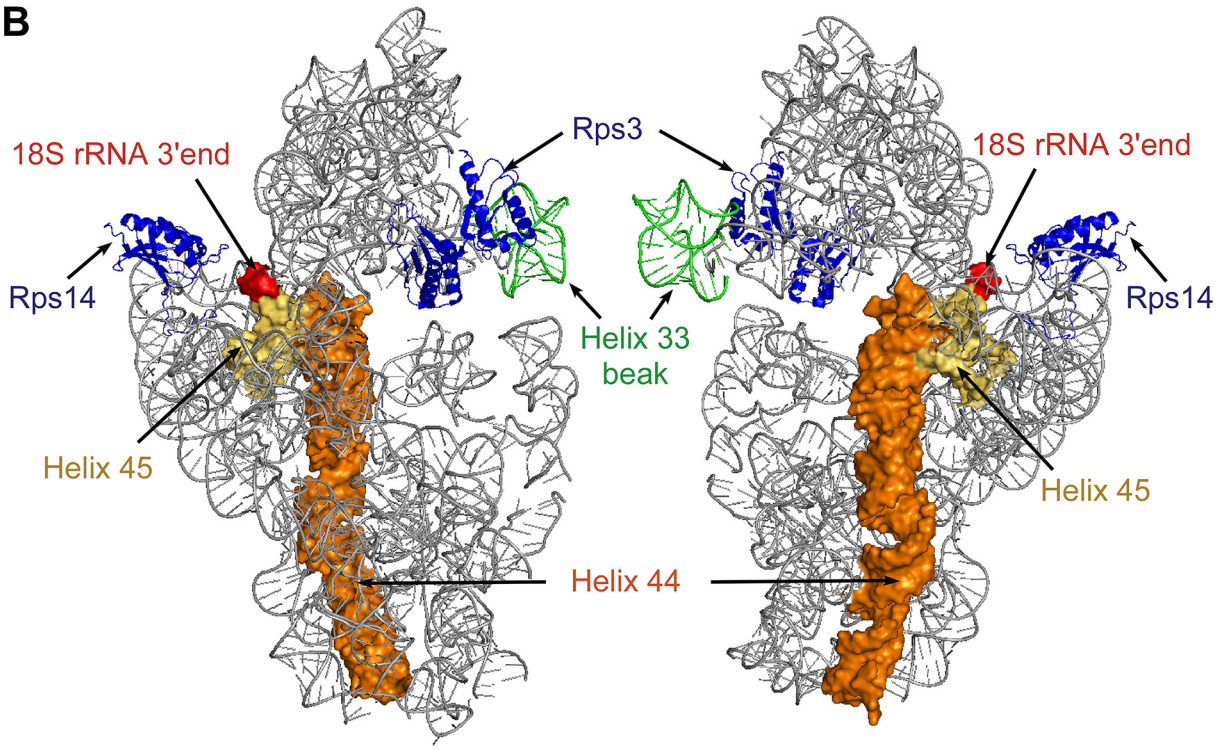
B
18S rRNA 3'end
Rps3
18S rRNA 3'end
Rps14
Rps14
Helix 33
beak
Helix 45
Helix 45
Helix 44

truncated versions. The two bands above 70 kDa were identified as Hsp70 contaminants (Fig. 7*A*).

As an *in vitro* substrate for Nob1, we synthesized an RNA oligonucleotide comprising the RNA sequence surrounding cleavage site D (expected cleavage between A^{18} and A^{19}). This was embedded in an artificial stem (Fig. 7*B*) to prevent 3′–5′ and 5′–3′ exonuclease degradation of the substrate and facilitate measurement of endonuclease activity. In addition, we synthesized the same RNA with a U17G point mutation at position −2 with respect to the predicted cleavage site (Fig. 7*B*). This mutation was previously shown to inhibit 20 S pre-rRNA processing *in vivo* (49).

Incubation of the 5′-radiolabeled RNA substrate with purified wild-type Nob1 in the presence of manganese resulted in one main product generated by cleavage between A^{18} and A^{19}, the precise location of site D *in vivo* (Fig. 7, *B* and *C*). Longer exposure revealed two additional cleavage products, corresponding to cleavage at A^{28} and A^{31} (Fig. 7, *B*, *D*, *E*, and *F*). Cleavage efficiency improved with increasing concentrations of manganese, with an optimal efficiency at 5 mM (Fig. 7C), whereas no cleavage was observed in the presence of magnesium (data not shown). The requirement for manganese is consistent with observations from other PIN domain proteins, which also need manganese for cleavage activity and show inhibition by (13–18) magnesium.

Importantly, no cleavage occurred when the same amount of purified Nob1-D15N mutant protein was used in the *in vitro* assay (Fig. 7*D*). Moreover, cleavage at the authentic site D was abolished when wild-type Nob1 was tested with the RNA substrate containing the U17G mutation. Instead, Nob1 cleaved at the alternative sites A^{28} and A^{31}. Interestingly, the sequence around A^{28} (UUAA) resembles that of the *bona fide* site D (Fig. 7, *B* and *D*). Cleavage at A^{28} was much stronger in the U17G substrate than in the wild-type substrate, suggesting that the altered structure at A^{28} (*e.g.* loss of the U^{17}-A^{28} base pairing) allows more efficient cleavage at this site. Weak cleavage at A^{31} was also visible with the U17G substrate. An explanation for the lower cleavage efficiency could be the different sequence before the cleavage site (AUAA, compared with UUAA at site D).

The yield of site D cleavage product was improved by increasing the amount of substrate or protein used (Fig. 7*E*), or extending the incubation time (Fig. 7*F*). However, saturation of the reaction was observed at elevated protein concentrations, suggesting that either the amount of correctly folded RNA substrate is limiting or that the RNA substrate is fully bound by Nob1, but only a small fraction of the protein is cleavage-competent (Fig. 7*E*).

Together, these data show that Nob1 purified from yeast exhibits endonuclease activity *in vitro* and cleaves a model substrate at the cleavage site D, demonstrating that Nob1 is indeed the D-site endonuclease.

To test if *in vivo* Nob1 has exerted its cleavage activity on 20 S pre-rRNA in late pre-40 S particles, with which it is associated, we analyzed the RNA content of the late pre-40 S particle affinity-purified via Ltv1-TAP (7). This nascent 40 S subunit contained Nob1 and 20 S pre-rRNA with little mature 18 S rRNA (Fig. 8, *A* and *B*). These data imply that, although Nob1 was present in the purified pre-40 S particle, it had not significantly cleaved the 20 S pre-rRNA either *in vivo* or during purification. This observation suggests that Nob1 endonuclease activity is under regulation in the pre-40 S particle (see "Discussion").

Suppression of the 20 S Pre-rRNA Processing Defect in the ltv1Δ pfa1Δ and ltv1Δ prp43–414 Mutants Requires the Endonuclease Activity of Nob1—To test whether the endonuclease activity of Nob1 is required for suppression of the phenotypes of *ltv1Δ pfa1Δ* and *ltv1Δ prp43–414* double mutants, we tested catalytically inactive Nob1-D15N. As anticipated, Nob1-D15N failed to suppress growth inhibition in the double mutants, although expression levels of mutant and wild-type Nob1 were similar (Fig. 9, *A* and *B*). Even when Nob1-D15N was overexpressed (either from the *ADH1* or *NOP1* promoter), no suppression was observed (data not shown). Moreover, expression of Nob1-E43Q or Nob1-D92N, which have mutations in other critical PIN domain residues (supplemental Fig. S4) (11) could neither complement the *nob1Δ* mutant nor suppress the growth defect of *ltv1Δ pfa1Δ* and *ltv1Δ prp43–414* double mutants (Fig. 9, *A* and *B*). Furthermore, an increased dosage of wild-type Nob1 but not of D15N, E43Q, or D92N mutant protein prevented accumulation of 20 S pre-rRNA and 17 S RNA in *ltv1Δ pfa1Δ* and *ltv1Δ prp43–414* mutants (Fig. 9*C*). These *in vivo* data demonstrate that the catalytic activity of Nob1 is essential for suppressing the 20 S pre-rRNA processing defect in *ltv1Δ pfa1Δ* and *ltv1Δ prp43–414* double mutants.

DISCUSSION

In this study, we identified a functional network linking the pre-40 S component Ltv1, the RNA helicase Prp43, the G-patch protein Pfa1, and the PIN domain protein Nob1. These function together in the processing of 20 S pre-rRNA to 18 S rRNA, which takes place in late, cytoplasmic pre-40 S subunits.

Up to now, the identity of the endonuclease catalyzing cytoplasmic D-site cleavage has been subject to speculation. Here, we developed an *in vitro* assay that faithfully reconstitutes Nob1-dependent endonuclease cleavage of a model substrate that mimics both the RNA sequence and the predicted secondary structure around cleavage site D of the 20 S pre-rRNA. Cleavage by Nob1 was specific because it mainly occurred at the predicted nucleotide, and cleavage at this model D-site was abolished by a single point mutation in the RNA substrate. The efficiency of cleavage was relatively low, perhaps reflecting the

FIGURE 10. **Structure of the 3′-end of the 18 S rRNA.** *A*, *left*, modeled secondary structure of the 18 S rRNA according to Refs. 54 and 55). Helix 33 is *encircled* in *green*. The *box* indicates the 3′ minor domain, consisting of helices 44 (*orange*) and 45 (*yellow*). *Right*, *enlarged view* of the 3′ minor domain. Binding sites of oligonucleotides 18 S 006 and 007 are indicated. The last nucleotide in the three-dimensional model shown in *B* and the actual 3′-end of the 18 S rRNA are displayed in *red*. The sequence of ITS1 within the predicted D-site hairpin (53) was added manually (*gray*). *B*, modeled structure of the yeast 40 S subunit, shown from the solvent (*left*) and intersubunit (*right*) sides. Helices 44 (*orange*) and 45 (*yellow*) corresponding to the last ~160 nucleotides at the 3′-end of the 18 S rRNA are shown as a *surface representation*. The 3′-end of the 18 S rRNA is displayed in *red*, and helix 33 is shown in *green*. Of the ribosomal proteins, only Rps3 and Rps14 are shown (*blue*). The displayed images were generated in PyMOL (DeLano Scientific).

absence of auxiliary factors and/or the context of the preribosome in the *in vitro* assay system. Consistent with both possibilities, isolated nascent pre-40 S subunits purified via Ltv1-TAP contain high amounts of unprocessed 20 S pre-rRNA, despite the presence of Nob1 (see Fig. 8, *A* and *B*). Thus, D-site cleavage by Nob1 may only be allowed to occur at a defined step late during the 40 S maturation pathway. Regulation of cleavage could be achieved either by directly controlling the activity of Nob1, by restricting the access of Nob1 to the substrate, or by controlling the conformation of the substrate. In all cases, additional factors would be required to accomplish such a regulation.

Our genetic screen isolated factors that are required for 20 S processing in addition to the Nob1 endonuclease. Mutations in *PRP43* and deletions of *PFA1* resulted in a dramatic accumulation of 20 S pre-rRNA, when combined with the *LTV1* deletion, indicating that Prp43, Pfa1, and Ltv1 are crucial for 20 to 18 S rRNA processing.

Despite the strong 20 S accumulation, the mutants were only slightly delayed in growth at higher temperatures, showing that high concentrations of 20 S pre-rRNA are not necessarily inhibitory to cell growth. This was supported by the co-sedimentation of 20 S pre-rRNA with polysomes in *ltv1*Δ *pfa1*Δ and *ltv1*Δ *prp43–414* double mutants, suggesting that 20 S pre-rRNA containing 40 S subunits can be tolerated in translating polysomes. This is in contrast to the wild-type strain and the *prp43–414*, *pfa1*Δ, and *ltv1*Δ strains, indicating that accumulated pre-40 S particles in the *ltv1*Δ *pfa1*Δ and *ltv1*Δ *prp43–414* double mutants are structurally different from the wild type or single mutants. Notably, co-sedimentation of 20 S pre-rRNA with polysomes was also described recently for an *rps31* mutant (50). Based on these observations, it is conceivable that 20 to 18 S rRNA processing might occur after 40 S-60 S subunit joining or even after the first round of translation. In *Dictyostelium*, only 40 S subunits that are capable of translation undergo the final rRNA processing step, providing a precedent (51).

Apart from the 20 S pre-rRNA, *ltv1*Δ *pfa1*Δ and *ltv1*Δ *prp43–414* mutants also accumulated 17 S RNA, a truncated version of the 18 S rRNA lacking ~160 nucleotides of the 3′-end (corresponding to rRNA helices 44 and 45 of the 18 S rRNA; see also Fig. 10, *A* and *B*), that is generated by the cytoplasmic exosome. This suggests that in *ltv1*Δ *pfa1*Δ and *ltv1*Δ *prp43–414* mutants, the 3′ region of the 20 S pre-rRNA, including helices 44 and 45 of the 18 S rRNA, is not protected from exonuclease attack. This further supports the idea that a structural difference may exist between the incompletely matured 40 S particles in *ltv1*Δ *pfa1*Δ and *ltv1*Δ *prp43–414* mutants and wild-type pre-40 S and mature 40 S subunits.

Notably, helix 44 contributes to the decoding site of 40 S subunits, which is critical for translational fidelity (52). An aberrant structure in this region could be deleterious to accurate translation, especially at low temperatures, when the rRNA is probably less flexible. Indeed, the *ltv1*Δ *pfa1*Δ and *ltv1*Δ *prp43–414* double mutants contained fewer polysomes and more 80 S monosomes at 23 than at 37 °C, suggesting that translation in the mutants is particularly impaired at lower temperatures (see also the distribution of 20 and 18 S rRNAs in the gradients; Fig. 6 and supplemental Fig. S2). Consistent with impaired translation, the *ltv1*Δ and *ltv1*Δ *pfa1*Δ strains showed increased sensitivity toward neomycin and paromomycin, both aminoglycosides known to bind to the upper part of helix 44.[5] The combination of inefficient translation with the increased accumulation of non-functional 17 S RNA provides an explanation for the stronger growth defects of the double mutants at low temperatures.

Our results show that Ltv1, Pfa1, and Prp43 are involved in 20 S processing, but in what way do they promote the endonucleolytic cleavage by Nob1? Since the rRNA processing defects in *ltv1*Δ *pfa1*Δ and *ltv1*Δ *prp43–414* mutants could be rescued by overexpression of the Nob1 endonuclease, the conditions for Nob1 RNA-substrate interaction or endonuclease activity are probably suboptimal in the *ltv1*Δ *pfa1*Δ and *ltv1*Δ *prp43–414* double mutants. These can, however, be compensated for by higher amounts of Nob1. This finding suggests that the correct functioning of Ltv1, Pfa1, and Prp43 is a prerequisite for efficient D-site cleavage by Nob1.

There is no evidence for a direct interaction between Nob1 and either Pfa1, Prp43, or Ltv1, making it unlikely that these proteins function as recruiting factors or allosteric activators of Nob1. We consider it more likely that Ltv1, Pfa1, and Prp43 regulate access of Nob1 to its substrate or prepare the substrate for efficient cleavage. In principal, this reorganization could take place in the nucleus. However, the finding that Ltv1, Pfa1, and Prp43 co-purify pre-40 S particles containing both 20 S pre-rRNA and 18 S rRNA makes it probable that they act in the cytoplasm, shortly before and during D-site cleavage (Fig. 8) (24).

A physical barrier preventing access of Nob1 to the cleavage site could be composed of either RNA or protein. A well characterized structural maturation step involving rRNA is exposure of helix 33 to generate the characteristic beak structure of the mature 40 S subunit. In the late pre-40 S particle, Ltv1 forms a complex with Enp1 and the ribosomal protein Rps3, which is implicated in this beak formation (7). In the modeled structure of the mature 40 S subunit, Rps3 is located close to the beak, suggesting that this is also likely to be the area where Ltv1 is bound (Fig. 10*B*). The position of helix 33 in the pre-40 S particle is not known; it is, however, possible that before being exposed to form the beak structure, this RNA is folded back on the particle and thereby hinders access of Nob1 to the cleavage site. The beak is formed concomitantly to or as a consequence of dissociation of Enp1 and Ltv1 from the particle (7). We speculate that this structural reorganization, which might be delayed in *ltv1* mutants, could be a prerequisite for 20 S cleavage by Nob1. Considering the major conformational rearrangement of rRNA that has to occur during beak formation, it is possible that also an RNA helicase is required for this process. In this case, Pfa1 and Prp43 might contribute together with Ltv1 to formation of the beak structure and thereby influence 20 S processing.

Our observation that in *ltv1*Δ *pfa1*Δ mutants, the 3′-end of the 18 S rRNA (corresponding to helices 44 and 45) is accessible to the exosome makes it, however, more likely that

[5] B. Pertschy, unpublished results.

this part of the rRNA is the direct target of Pfa1-Prp43. The action of these two proteins might be required to generate a stably structured, nuclease-resistant 3′-end of the 18 S rRNA. This idea is strongly supported by cross-linking experiments, which show that Prp43 binds to the 18 S rRNA at the base of helix 44, very close to cleavage site D (39). We speculate that the helicase activity of the Pfa1-Prp43 heterodimer acts to remodel the 18 S rRNA around helices 44 and/or 45 in order to prepare the RNA for cleavage by Nob1. Such a remodeling could be achieved by directly restructuring the rRNA but could also include the release of proteins bound in this region that might otherwise block access of Nob1 to the cleavage site.

We propose a model in which cytoplasmic 20 to 18 S rRNA processing is promoted by a number of interdependent steps: (i) beak formation and the respective structural rearrangement of the pre-40 S subunit, (ii) local restructuring of RNA helix 44 and/or 45 by Prp43-Pfa1 to allow access to cleavage site D, and (iii) cleavage at site D by the endonuclease Nob1. The combination of *in vitro* endonuclease assays with genetic analyses should allow the dissection of late steps in rRNA processing and their coordination with structural rearrangements.

Acknowledgments—We thank Dieter Kressler and Beate Schwer for providing plasmids. We also acknowledge the technical assistance of P. Ihrig and J. Reichert under the supervision of J. Lechner (Mass Spectrometry Unit, BZH Heidelberg). We thank D. Roser, D. Kressler, S. Ferreira-Cerca, A. Köhler, M. Skruzny, and H. Bergler for fruitful discussions.

REFERENCES

1. Fatica, A., and Tollervey, D. (2002) *Curr. Opin. Cell Biol.* **14,** 313–318
2. Fromont-Racine, M., Senger, B., Saveanu, C., and Fasiolo, F. (2003) *Gene* **313,** 17–42
3. Granneman, S., and Baserga, S. J. (2004) *Exp. Cell Res.* **296,** 43–50
4. Henras, A. K., Soudet, J., Gérus, M., Lebaron, S., Caizergues-Ferrer, M., Mougin, A., and Henry, Y. (2008) *Cell Mol. Life Sci.* **65,** 2334–2359
5. Tschochner, H., and Hurt, E. (2003) *Trends Cell Biol.* **13,** 255–263
6. Seiser, R. M., Sundberg, A. E., Wollam, B. J., Zobel-Thropp, P., Baldwin, K., Spector, M. D., and Lycan, D. E. (2006) *Genetics* **174,** 679–691
7. Schäfer, T., Maco, B., Petfalski, E., Tollervey, D., Böttcher, B., Aebi, U., and Hurt, E. (2006) *Nature* **441,** 651–655
8. Venema, J., and Tollervey, D. (1999) *Annu. Rev. Genet.* **33,** 261–311
9. Granneman, S., Nandineni, M. R., and Baserga, S. J. (2005) *Mol. Cell. Biol.* **25,** 10352–10364
10. Fatica, A., Oeffinger, M., Dlakiæ, M., and Tollervey, D. (2003) *Mol. Cell. Biol.* **23,** 1798–1807
11. Fatica, A., Tollervey, D., and Dlakiæ, M. (2004) *RNA* **10,** 1698–1701
12. Schäfer, T., Strauss, D., Petfalski, E., Tollervey, D., and Hurt, E. (2003) *EMBO J.* **22,** 1370–1380
13. Schneider, C., Leung, E., Brown, J., and Tollervey, D. (2009) *Nucleic Acids Res.* **37,** 1127–1140
14. Schaeffer, D., Tsanova, B., Barbas, A., Reis, F. P., Dastidar, E. G., Sanchez-Rotunno, M., Arraiano, C. M., and van Hoof, A. (2009) *Nat. Struct. Mol. Biol.* **16,** 56–62
15. Skruzný, M., Schneider, C., Rácz, A., Weng, J., Tollervey, D., and Hurt, E. (2009) *PLoS Biol.* **7,** e8
16. Lebreton, A., Tomecki, R., Dziembowski, A., and Séraphin, B. (2008) *Nature* **456,** 993–996
17. Eberle, A. B., Lykke-Andersen, S., Mühlemann, O., and Jensen, T. H. (2009) *Nat. Struct Mol. Biol.* **16,** 49–55
18. Huntzinger, E., Kashima, I., Fauser, M., Saulière, J., and Izaurralde, E. (2008) *RNA* **14,** 2609–2617
19. Bleichert, F., and Baserga, S. J. (2007) *Mol. Cell* **27,** 339–352
20. Bohnsack, M. T., Kos, M., and Tollervey, D. (2008) *EMBO Rep.* **9,** 1230–1236
21. de la Cruz, J., Kressler, D., Tollervey, D., and Linder, P. (1998) *EMBO J.* **17,** 1128–1140
22. Kos, M., and Tollervey, D. (2005) *Mol. Cell* **20,** 53–64
23. Weaver, P. L., Sun, C., and Chang, T. H. (1997) *Mol. Cell. Biol.* **17,** 1354–1365
24. Lebaron, S., Froment, C., Fromont-Racine, M., Rain, J. C., Monsarrat, B., Caizergues-Ferrer, M., and Henry, Y. (2005) *Mol. Cell. Biol.* **25,** 9269–9282
25. Janke, C., Magiera, M. M., Rathfelder, N., Taxis, C., Reber, S., Maekawa, H., Moreno-Borchart, A., Doenges, G., Schwob, E., Schiebel, E., and Knop, M. (2004) *Yeast* **21,** 947–962
26. Longtine, M. S., McKenzie, A., 3rd, Demarini, D. J., Shah, N. G., Wach, A., Brachat, A., Philippsen, P., and Pringle, J. R. (1998) *Yeast* **14,** 953–961
27. Puig, O., Caspary, F., Rigaut, G., Rutz, B., Bouveret, E., Bragado-Nilsson, E., Wilm, M., and Séraphin, B. (2001) *Methods* **24,** 218–229
28. Kressler, D., Doère, M., Rojo, M., and Linder, P. (1999) *Mol. Cell. Biol.* **19,** 8633–8645
29. Grosshans, H., Hurt, E., and Simos, G. (2000) *Genes Dev.* **14,** 830–840
30. Kressler, D., de la Cruz, J., Rojo, M., and Linder, P. (1997) *Mol. Cell. Biol.* **17,** 7283–7294
31. Bassler, J., Grandi, P., Gadal, O., Lessmann, T., Petfalski, E., Tollervey, D., Lechner, J., and Hurt, E. (2001) *Mol. Cell* **8,** 517–529
32. Yaffe, M. P., and Schatz, G. (1984) *Proc. Natl. Acad. Sci. U.S.A.* **81,** 4819–4823
33. Simos, G., Segref, A., Fasiolo, F., Hellmuth, K., Shevchenko, A., Mann, M., and Hurt, E. C. (1996) *EMBO J.* **15,** 5437–5448
34. Mitchell, P., Petfalski, E., and Tollervey, D. (1996) *Genes Dev.* **10,** 502–513
35. Arenas, J. E., and Abelson, J. N. (1997) *Proc. Natl. Acad. Sci. U.S.A.* **94,** 11798–11802
36. Martin, A., Schneider, S., and Schwer, B. (2002) *J. Biol. Chem.* **277,** 17743–17750
37. Combs, D. J., Nagel, R. J., Ares, M., Jr., and Stevens, S. W. (2006) *Mol. Cell. Biol.* **26,** 523–534
38. Leeds, N. B., Small, E. C., Hiley, S. L., Hughes, T. R., and Staley, J. P. (2006) *Mol. Cell. Biol.* **26,** 513–522
39. Bohnsack, M. T., Martin, R., Granneman, S., Ruprecht, M., Schleiff, E., and Tollervey, D. (2009) *Mol. Cell.*, in press
40. Boon, K. L., Auchynnikava, T., Edwalds-Gilbert, G., Barrass, J. D., Droop, A. P., Dez, C., and Beggs, J. D. (2006) *Mol. Cell. Biol.* **26,** 6016–6023
41. Tanaka, N., Aronova, A., and Schwer, B. (2007) *Genes Dev.* **21,** 2312–2325
42. Tsai, R. T., Tseng, C. K., Lee, P. J., Chen, H. C., Fu, R. H., Chang, K. J., Yeh, F. L., and Cheng, S. C. (2007) *Mol. Cell. Biol.* **27,** 8027–8037
43. Aravind, L., and Koonin, E. V. (1999) *Trends Biochem. Sci.* **24,** 342–344
44. Jakovljevic, J., de Mayolo, P. A., Miles, T. D., Nguyen, T. M., Léger-Silvestre, I., Gas, N., and Woolford, J. L., Jr. (2004) *Mol. Cell.* **14,** 331–342
45. Stevens, A., Hsu, C. L., Isham, K. R., and Larimer, F. W. (1991) *J. Bacteriol.* **173,** 7024–7028
46. Anderson, J. S., and Parker, R. P. (1998) *EMBO J.* **17,** 1497–1506
47. Araki, Y., Takahashi, S., Kobayashi, T., Kajiho, H., Hoshino, S., and Katada, T. (2001) *EMBO J.* **20,** 4684–4693
48. Houseley, J., and Tollervey, D. (2009) *Cell* **136,** 763–776
49. van Beekvelt, C. A., Jeeninga, R. E., van't Riet, J., Venema, J., and Raué, H. A. (2001) *RNA* **7,** 896–903
50. Lacombe, T., García-Gómez, J. J., de la Cruz, J., Roser, D., Hurt, E., Linder, P., and Kressler, D. (2009) *Mol. Microbiol.* **72,** 69–84
51. Mangiarotti, G., Chiaberge, S., and Bulfone, S. (1997) *J. Biol. Chem.* **272,** 27818–27822
52. Ogle, J. M., Brodersen, D. E., Clemons, W. M., Jr., Tarry, M. J., Carter, A. P., and Ramakrishnan, V. (2001) *Science* **292,** 897–902
53. Yeh, L. C., Thweatt, R., and Lee, J. C. (1990) *Biochemistry* **29,** 5911–5918
54. Spahn, C. M., Beckmann, R., Eswar, N., Penczek, P. A., Sali, A., Blobel, G., and Frank, J. (2001) *Cell* **107,** 373–386
55. Cannone, J. J., Subramanian, S., Schnare, M. N., Collett, J. R., D'Souza, L. M., Du, Y., Feng, B., Lin, N., Madabusi, L. V., Müller, K. M., Pande, N., Shang, Z., Yu, N., and Gutell, R. R. (2002) *BMC Bioinformatics* **3,** 2